Eur. Phys. J. D (2017) 71: 106
DOI: 10.1140/epjd/e2017-70740-7

THE EUROPEAN PHYSICAL JOURNAL D

Regular Article

Rotationally inelastic cross sections, rates and cooling times for para-H_2^+, ortho-D_2^+ and HD^+ in cold helium gas*

Mario Hernández Vera[1], Stephan Schiller[2], Roland Wester[1], and Francesco Antonio Gianturco[1,a]

[1] Institut für Ionenphysik und Angewandte Physik, Universität Innsbruck, Technikerstr. 25/3, 6020 Innsbruck, Austria
[2] Institut für Experimentalphysik, Heinrich-Heine Universität Düsseldorf, Universtätsstr. 1, 40225 Düsseldorf, Germany

Received 27 November 2016
Published online 18 May 2017

Abstract. In the present work we discuss the dynamical processes guiding the relaxation of the internal rotational energy of three diatomic ions, the para-H_2^+, the ortho-D_2^+ and the HD^+ in collision with He atoms. The state-changing cross sections and rates for these Molecular Hydrogen Ions (MHIs) are obtained from Close Coupling quantum dynamics calculations and the decay times into their respective ground states are computed by further solving the relevant time-evolution equations. The comparison of the results from the three molecules allows us to obtain a detailed understanding, and a deep insight, on the relative efficiencies of the relaxation processes considered.

1 Introduction

The marked improvements on the performances of the field of cold chemistry research which have occurred in the last few years have allowed an increasingly wider range of studies for ion-neutral chemical processes involving charge-exchange chemistry [1,2] and radiative association mechanisms [3]. They have also made possible to explore the possibility of observing state-selected chemistry [4] or of doing the spectroscopic analysis of trapped-molecular ions under cold conditions [5,6].

When molecular systems are studied in this way, the uploading of a buffer gas, e.g. He, will cause in-trap collisions that will couple translational degrees of freedom to the internal states of the molecular partners through the spatial anisotropy of the interaction's potential energy surfaces (PES) between the partners in the trap. Such a picture also requires defining a "cold" He partner, a feature of the present processes that we shall further discuss later on: its translational temperature will be assumed to be experimentally settable in the range between 4 K and 300 K and will therefore be treated as an adjustable parameter during the calculations [7–9].

The collisional energy transfer will therefore provide an important path to finally produce thermally cold partners which are also in the ground-states of all the molecular ion's forms of internal energy (electronic, vibrational, and rotational), with the exclusion in the present study of "spin energy" changes. This means that the molecular interaction between the buffer gas and the molecular ions shall provide the main driving force for the internal thermalisation of the molecular ions.

For the cases that we shall study in the present work, i.e. three molecular hydrogen ions (MHIs): para-H_2^+, ortho-D_2^+ and HD^+, there is an additional interest provided by the fact that such conceptually simple one-electron molecules can be also used as testing ground of fundamental physics [10]. In all the above examples it is useful, and possibly essential, to actually manipulate their internal states in order to provide, in the end, translationally cooled molecules which have also reached their lowest rovibrational states. Thus, one can achieve in principle a high population of the trapped ions into their $|\nu = 0, N = 0\rangle$ vibrational-rotational internal states for further experimental tests [11].

Since two of the molecules which we intend to study have no permanent dipole moments, radiative manipulation into their lowest internal states is not a viable path, while being a possibility for HD^+ [12]. It therefore follows that collisional cooling of the homonuclear MHIs is the primary way through which the manipulation into the $|\nu = 0, N = 0\rangle$ state can be achieved, while it remains also an interesting process to explore for the HD^+ isotopic variant in competition with the radiative energy transfer channels.

More specifically, the task of buffer-gas cooling of the MHIs in a cold ion trap is to prepare the para-H_2^+, the ortho-D_2^+ and the HD^+ in their $|\nu = 0, N = 0\rangle$ lowest rovibrational states. We shall not be considering, for now, the effects from spin-rotation coupling (all the MHIs are in their $^2\Sigma_g^+$ electronic ground state) and the further

* Contribution to the Topical Issue "Dynamics of Molecular Systems (MOLEC 2016)", edited by Alberto Garcia-Vela, Luis Banares and Maria Luisa Senent.

[a] e-mail: francesco.gianturco@uibk.ac.at

level splitting effects caused by hyperfine structure coupling. The reason for this is based on our recent computational study on the para-H_2^+ and ortho-H_2^+ molecules, [13] rotational state-changing collision cross sections that was carried out within a range of relevant temperatures for trap manipulation. In that work, we performed exact quantum dynamical calculations of rotationally inelastic collisions for both partners interacting with He atom and employed the full formulation using the relevant level splitting effects mentioned above. We further repeated the calculations without the level splitting effects and treating the target ions as simpler targets in pseudo-$^1\Sigma$ states: the results were nearly coincident with the sums of all the components cross sections obtained first from using the correct coupling during the scattering calculations. In the analysis that we shall present below all three of them were therefore treated by using the simpler picture of the three target molecules in their pseudo-$^1\Sigma$ electronic states. In the examples below we shall still consider the consequences of the symmetrization postulate and limit our comparison to that between homonuclear isotopic species with even rotational quantum numbers.

From the computed cross sections we further generated the state-to-state rate constants needed for the time-evolution study of the title systems.

In Section 2 we provide an outline of the potential energy surfaces (PESs) that we have employed for our calculations, while Section 3 will briefly outline our quantum scattering calculations and discuss the results for the state-changing rotationally inelastic cross sections. The latter dynamical observables will then go into producing the necessary array of elastic and inelastic rates for all three cases of MHIs discussed in our work: we shall present and discuss them in Section 4. The following section will present the coupled first-order homogeneous equations employed to analyse the time evolution of the three molecular systems under trap conditions and produce specific values for their relative cooling times in the presence of the buffer gas. Our present conclusions will be reported in the last Section 5.

2 Computed interaction potential energy surfaces for the MHIs with He

The interaction between an He atom and the H_2^+ molecule has been studied and computationally modelled several times over the years. One of the earlier, among the fairly recent accurate treatments, was due to Falcetta and Siska [14], who carried out an extensive quantum chemistry calculations of the 3D problem of the lowest electronic state potential $V(r, R, \theta)$, where r is the intramolecular bond distance, R the distance between the He atom and the center-of-mass in the target ion, and θ the angle between the two vectors associated with the (r, R) coordinates.

A more extensive calculation was produced for the same H_2He^+ system, with the aim of describing that interaction in terms of its chemical coordinates (R_1, R_2, R_3),

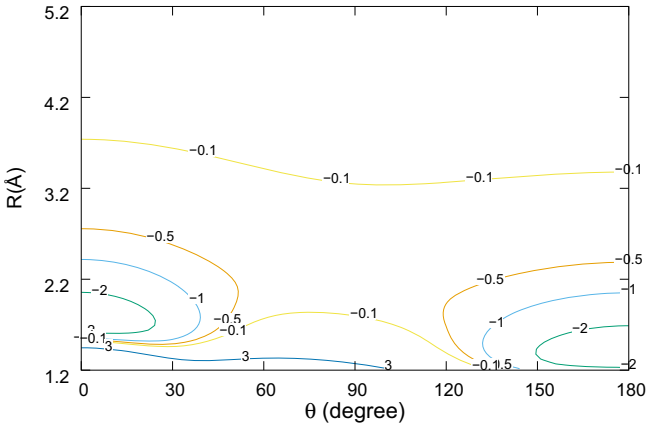

Fig. 1. PES for the He-HD^+ system (Vibrationally Averaged). The H-D bond has the H-side at 180°. Energies are in units of 10^3 cm^{-1}.

the latter being the interatomic distances between the three partner atoms [15,16]. We have further employed the calculations of reference [16] to extract the potential energy surface for H_2^+, D_2^+ and HD^+ in terms of the same dynamical coordinates discussed in the earlier work by Falcetta and Siska [14] and already defined before. We additionally formulate that potential function in terms of the conventional multipolar coefficients originated by an expansion over Legendre orthogonal polynomials

$$V(R, \theta, r) = \sum_{\lambda=0}^{\lambda_{max}} V_\lambda(R, r) P_\lambda(\cos\theta) \qquad (1)$$

and have found that the expansion coefficients numerically converge by including terms up to $\lambda_{max} = 20$, although the lowest five coefficients are the dominant ones at the present collision energies. All the details of the expansion of equation (1) were extensively discussed and analyzed in reference [13] and will not be repeated here. We have also carried out a detailed comparison of our present choice for the non-reactive PES with additional earlier calculations (which turned out to be very similar to our present choice) in another, separate publication from our group [17]. Suffice it to say that our present choice of the interaction potential agrees closely with all the most recent evaluations of the same PES and indicates the accurate quality of the description of it which we have employed in the present work.

Turning now to the PES features in the specific case of the HD^+ system, we report in Figure 1 the iso-energy curves of the He/HD^+ PES. The two-dimensional PES was obtained from the full three-dimensional PES by averaging over the intermolecular ground-state vibrational wavefunction, a procedure we had previously called the Vibrationally Averaged (VA) final interaction potential for the case of the target's ground vibrational state. For further details see again reference [17] that reports our detailed comparison of the most recent PESs for the present MHI targets.

One clearly sees that the mass difference between the proton and deuteron causes an asymmetry in the two

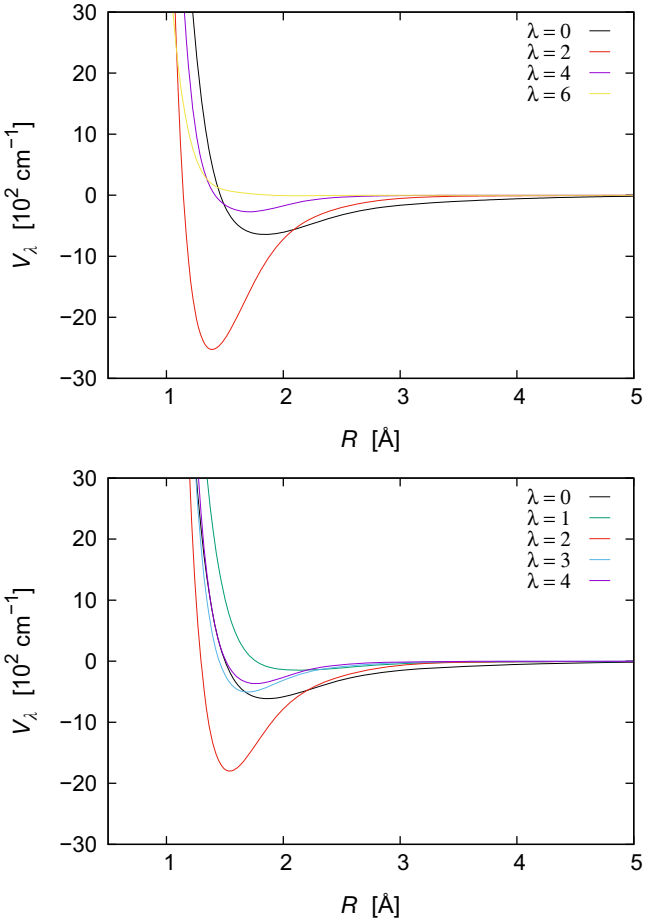

Fig. 2. Radial coefficients of the Legendre expansion of equation (1) for the PES corresponding to the H_2^+/He (upper panel) and the HD^+/He (lower panel).

potential wells located along the collinear geometry, in this case shifted by the induced shift of the center of mass position. The energy isolines indicate that on the H-side the He projectile gets closer to the molecular repulsive wall than on the D-side of the molecule. The corresponding PES surfaces for the H_2^+/D_2^+ systems show instead the expected symmetry on the two sides of approach, not shown in this work but discussed elsewhere [17] in greater detail.

Another interesting way of showing the differences, and also the fundamental similarities, of the two homonuclear MHIs with respect to the HD^+, can be seen from a comparison of the radial coefficients of the Legendre expansion of the PES. They are reported in the two panels of Figure 2. The upper panel shows the even-numbered coefficients for the H_2^+/He system, while the lower panel reports the coefficients for the HD^+/He system. Both molecules are kept at their equilibrium molecular geometry (i.e. without the vibrational averaging we mentioned above).

The following considerations can be made by comparing the radial coefficients in the two panels:

(i) for both systems the strongest anisotropic coefficient occurs for $\lambda = 2$, where in both cases rather marked wells appear at short range;

(ii) the HD^+ target molecule exhibits the outermost onset of its repulsive wall, acting in the low-energy range of collisions which are relevant to this study, for the $\lambda = 1$ anisotropic potential. This feature suggesting that the $\Delta j = 1$ transitions will also be as important as those driven by the $\lambda = 2$ coupling potential multipole component. Here the label j defines the simplified (see previous discussion) rotational quantum number for the states of the molecular ions;

(iii) the homonuclear case, on the other hand, shows its $\lambda = 4$ anisotropic coefficient to present the outermost location of the repulsive wall at low collision energies. It will therefore show the $\Delta j = 4$ transitions to be as important as those for $\Delta j = 2$, as we shall further discuss below in the next section, since the odd multipolar coefficients are here absent.

3 The multichannel quantum scattering dynamics: a brief outline

To solve the problem of the rotational quenching dynamics corresponds to solving the time-independent Schrödinger equation (TISE) for the nuclei that move on the potential energy surface defined by equation (1), enforcing on their motion the usual asymptotic scattering boundary conditions [18]. Our numerical strategy to the solution of the TISE is the coupled channel approach (CC) as implemented in our in-house developed scattering code ASPIN [19]. Details of the method have been given before [18,19] and therefore will not be reported in the present paper. They were already discussed recently in detail for the case of para-H_2^+/He system [13].

It is worth noting now that for the present systems all the angular momentum couplings are fully accounted for by our CC description of the nuclear dynamics and hence the calculations of the rotational quenching process given by our computational model can be considered as basically exact, within the accuracy of the employed PES. The molecular basis set consists of 1 vibrational state, which we have employed to generate the initial vibrationally averaged anisotropic PES, and 20 rotational functions for each of the target ions which have been used in the asymptotic channel expansions.

The $\sigma_J(j_i \rightarrow j_f|E)$ partial integral cross sections have been carefully checked for convergence against the basis set size and propagator parameters and it is well within 1%. In particular, we have propagated the solution from $R = 1.0$ Å to $R = 50.0$ Å with 500 steps of the LogDer propagator [20]. The convergence of the sums on the partial cross-sections to obtain the corresponding state-to-state integral cross sections was also controlled by extending the J values up to at least $J_{max} = 80$.

As we chiefly wish to describe the rotational quenching process, we are principally interested in the (de-)excitation transition cross sections between different rotational states within the same vibrational level: $(\nu_0, j = j_i) \rightarrow (\nu_0, j = j_f)$, with ν_0 indicating the vibrational ground state of the MHI target ion. For the sake of notation clarity,

Table 1. Comparison between cross sections computed with the pseudo-$^1\Sigma$ approximation and the corresponding cross sections as sums over fine levels for p-H_2^+. Here we only present transitions between fine rotational levels with $j = N + 1/2$.

Transitions	$E = 10$ cm^{-1}		$E = 20$ cm^{-1}		$E = 50$ cm^{-1}		$E = 100$ cm^{-1}	
$N \to N'$	$\sigma_{N\to N'}$	$\sum_{j'} \sigma_{N_j \to N'_{j'}}$	$\sigma_{N\to N'}$	$\sum_{j'} \sigma_{N_j \to N'_{j'}}$	$\sigma_{N\to N'}$	$\sum_{j'} \sigma_{N_j \to N'_{j'}}$	$\sigma_{N\to N'}$	$\sum_{j'} \sigma_{N_j \to N'_{j'}}$
$2 \to 0$	26.645	31.798	21.214	23.147	14.414	15.685	8.716	9.424
$4 \to 0$	7.172	7.886	6.779	7.266	4.175	4.471	3.011	3.197
$4 \to 2$	61.926	67.239	48.817	52.263	34.900	37.061	25.199	26.594
$6 \to 2$	21.667	23.318	19.739	21.108	16.477	17.304	12.080	12.671
$6 \to 4$	93.532	101.641	73.634	77.727	46.262	48.641	27.901	29.469

in the following formulas we assume implicitly that the system is always in its vibrational ground state, ν_0.

As discussed in a separate publication, we first obtained final cross sections values using the full dynamical accounting of the fine-structure coupling of angular momenta. Their values turned out to be close to those obtained using simplified CC calculations that treat the target molecular ions as pseudo-$^1\Sigma^+$ states [13]. An example of the actual differences between the two sets of calculations is reported by the data of Table 1. We show there, over a fairly broad range of collision energies, the CC calculations that use the pseudo-$^1\Sigma$ treatment of the rotating target (left-side column at each chosen energy) and the results from using the full fine-structure coupling of angular momenta (right-side columns).

The larger differences between cross section values appear at the lowest energies, while becoming clearly smaller as we move to the larger collision energies. In any event, such differences are in most cases less than or around 10% and therefore suggest that in the present study we could more efficiently use the simplified coupling scheme of angular momenta without a strong modification of the final rates values used in the present comparison. Thus, to generate the ensuing state-to-state collisional rates at the relevant temperatures for the ion trap modeling, we decided that it was accurate enough to employ the pseudo-$^1\Sigma$ dynamical coupling for all the MHI targets colliding with He atoms.

In terms of the notation we have used, one should be reminded that within the full fine-structure coupling the total angular momentum is defined as a sum of vectors: $\mathbf{j} = \mathbf{N} + \mathbf{S}$. Hence, in the simplified notation of the pseudo-$^1\Sigma$ we should have that $\mathbf{j} = \mathbf{N}$ and therefore all transitions within the pseudo-$^1\Sigma$ should be labelled, as done in Table 1, as $N \to N'$ transitions. However, to avoid possible confusion we have mantained the same notation throughout the paper while reminding the reader that for all data obtained within the pseudo-$^1\Sigma$ treatment of the dynamics the physical meaning of $\mathbf{j}$ has changed from the exact sum of vectors $\mathbf{j} = \mathbf{N} + \mathbf{S}$ to the simpler $\mathbf{j} = \mathbf{N}$.

Once the integral cross sections are known, the rotationally inelastic rate constants, $k_{j\to j'}(T)$ can be evaluated as the convolution of the computed total partial cross sections over a Boltzmann distribution of relative collision energies. In the equation below all quantitites are given in

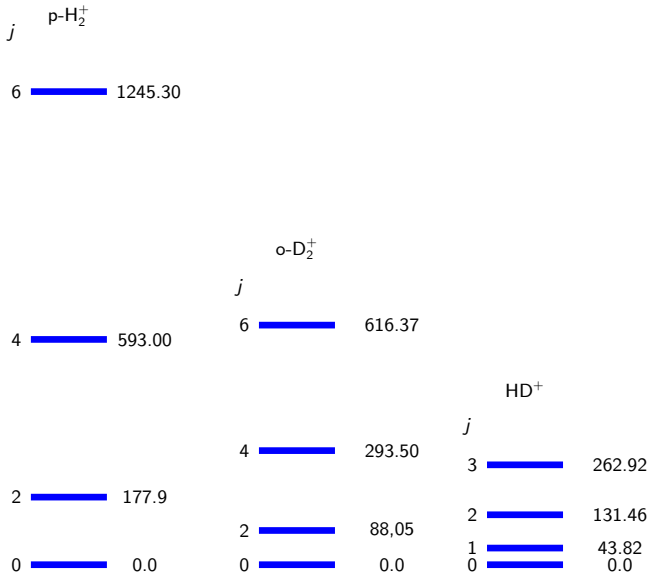

Fig. 3. Rotational energies (in cm^{-1}) for the first four rotational levels of all three molecules discussed in the present work. All levels are given within the pseudo-$^1\Sigma$ reduced coupling scheme (see main text for details). The rotational constants employed are: 29.65 cm^{-1} for H_2^+, 14.675 cm^{-1} for D_2^+ and 21.91 cm^{-1} for HD^+.

atomic units:

$$k_{j\to j'}(T) = \left(\frac{8}{\pi\mu k_B^3 T^3}\right)^2 \times \int_0^\infty E\sigma(j \to j')(E)e^{-E/k_B T}dE. \quad (2)$$

To better clarify the energy transfer processes involved in each of the ionic target, treated as simpler rigid rotors, we present the energy levels of the lower rotational states in Figure 3. The rotational constants used in this figures and in our scattering calculations for H_2^+, D_2^+ and HD^+ were taken from references [14,21,22], respectively.

The largest energy spacings are for the lightest target, the p-H_2^+ molecular ion: its first four levels up to $j = 6$ span more than 1200 cm^{-1}, while the heaviest isotope spans only about half that energy range. The structure of the HD^+ is such that the first four rotational levels

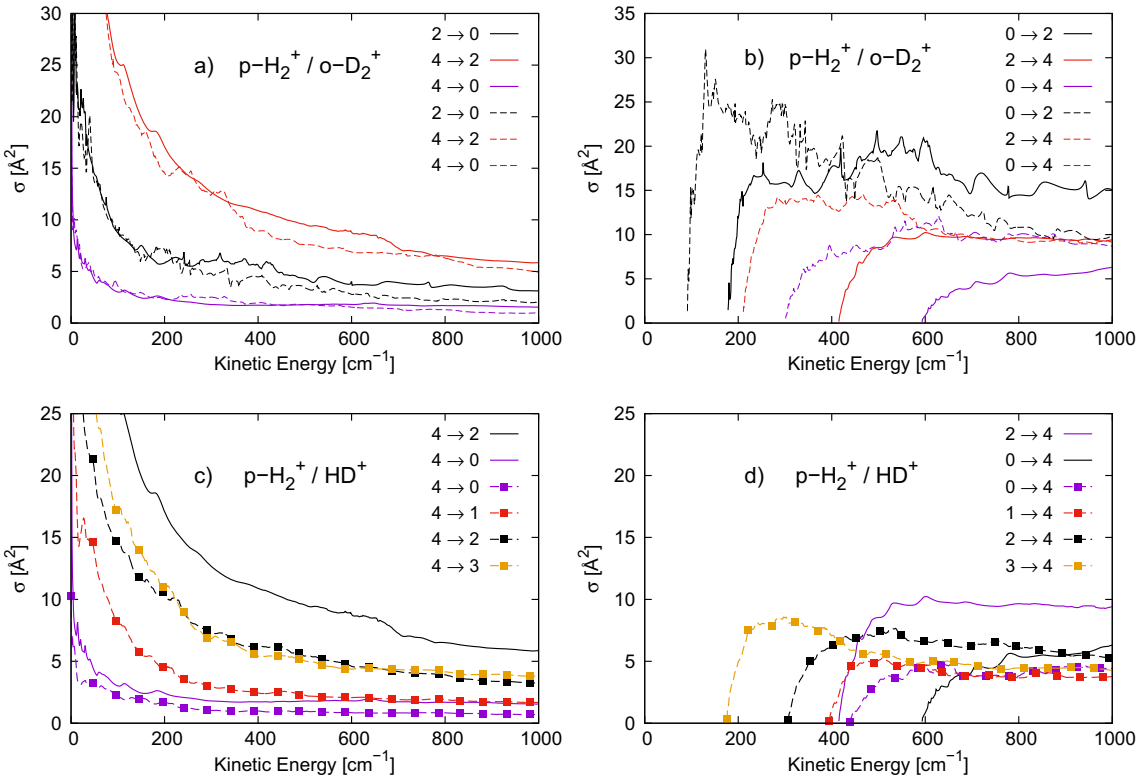

Fig. 4. Collisional kinetic energy dependence of the rotationally inelastic cross sections. (a), (c): Comparison of the de-excitation cross sections between p-H_2^+ (continuous lines) and o-D_2^+ (dashed lines). (b), (d): Comparison of the excitation cross sections between p-H_2^+ (continuous lines) and HD^+ (dashed lines with squares).

only span about 260 cm^{-1}, i.e. less than 1/4th of its lighter counterpart. Such differences will be reflected in the strength and size of the computed state-changing cross sections that we shall be presenting in the next section.

4 The computed inelastic cross sections and rate coefficients

Following the numerical indicators that we have already mentioned in the previous section, we have obtained an extensive network of inelastic and elastic cross sections relevant for the relaxation processes we intend to model in the present work.

In Figure 4 we report our comparison between excitation and de-excitation cross sections for all three MHIs discussed in the present work.

The following comments could be made from the four panels of Figure 4:

(i) In the case of H_2^+ in comparison with D_2^+, we see clearly that the opposite roles of energy spacings (which favour the heavier isotope because of reduced energy gaps) and of kinematic effects (which would favour instead a larger collisional efficiency for the lighter isotope in relation with the same He projectile) produce in the end very similar de-excitation cross sections for these two systems, as seen in Figure 4a.

(ii) When looking at the excitation cross sections, in Figure 4b, we further note that the excitation processes for the heavier isotopic variant have their opening thresholds at lower energies and therefore they dominate the state-changing efficiency up to about 180 cm^{-1}. At this energy, however, the excitation collisions for H_2^+ start to contribute and maintain similar strength at all the considered energy, as it occurred for the de-excitation processes.

(iii) The corresponding comparison between de-excitation cross sections for the lightest homonuclear system and the dipolar isotope HD^+ is presented in Figure 4c. We see there that the largest cross sections in the homonuclear case pertain to the $(4 \rightarrow 2)$ de-excitation process, a dynamical mechanism dominated by the $\lambda = 2$ and $\lambda = 4$ anisotropic coefficients of equation (1). On the other hand, the lower symmetry of the HD^+ target allows the latter transition to share de-excitation flux with the $(4 \rightarrow 3)$ process and therefore HD^+ produces two comparable cross sections for such processes, albeit getting them smaller than the similar de-excitation channel in Figure 4c for H_2^+. All the inelastic cross sections shown in that panel, however, indicate the HD^+ target as yielding uniformly smaller values in comparison with H_2^+.

(iv) Figure 4d reports comparisons between excitation processes for H_2^+ and HD^+. The large differences in the level spacings discussed earlier are clearly shown

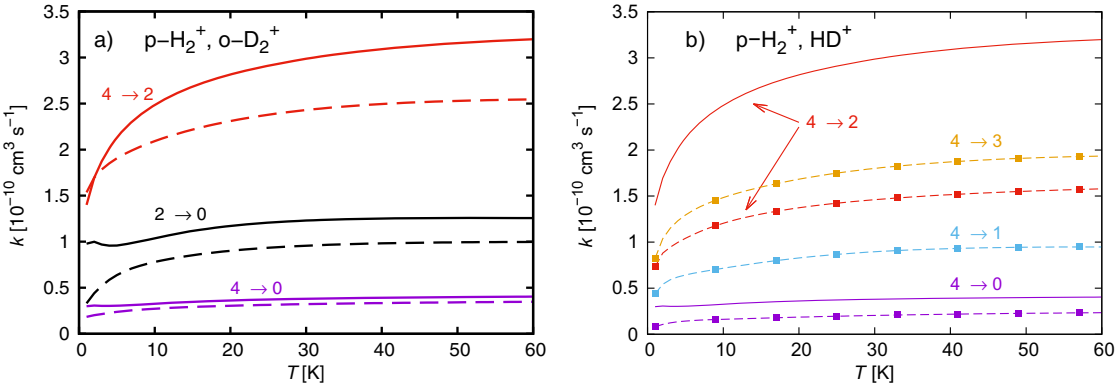

Fig. 5. Inelastic rate coefficients as a function of the collisional temperature. Panel (a): comparison of the de-excitation rates between p-H_2^+ (continuous line) and o-D_2^+ (dotted lines). Panel (b): comparison of the de-excitation rates between p-H_2^+ (continuous line) and HD^+ (dashed lines with squares).

by the start of the HD^+ rotational excitation collisions at much lower relative energies. Furthermore, we see that the $\Delta j = 1$ selection rule for the polar molecule shows up again by producing for such processes cross sections which are similar in size with those associated with the $\Delta j = 2$ transitions: the different symmetries of the multipolar coefficients between the two target ions therefore control the relative sizes of the corresponding cross sections.

(v) In both sets of inelastic cross sections reported for excitations (right-hand panels) and de-excitation (left-hand panels) one notices that a great deal of resonant structures are present near the collision energy thresholds for each process considered. This is not surprising since the ionic interactions, as shown in the earlier section, are indeed rather strong with fairly deep attractive wells: all features which point at the possibility of resonant trapping of the He atoms when the collision enegies are small and relatively large amount of energy is being transferred during collisions. Furthermore, the presence of at least two closed channels needed to attain numerical convergence also suggest that Feshbach-type resonances are also possible. Since our present study intends to chiefly deal with the comparison of relaxation times as provided by a kinetic analysis of the relative inelastic rates, we decided that a closer analysis of the resonances would be outside the scope of the present work.

The relative behavior of the inelastic cross sections discussed above is also reflected in the rotationally inelastic rate coefficients. They have been computed following equation (2) and over a much larger array of inelastic cross sections than those shown in Figure 5: the latter are some examples selected for the present discussion.

The results reported in the left panel show a comparison between the de-excitation rate coefficients for the p-H_2^+ target ion and those for the heaviest isotopic variant, given by dotted lines. The examples we give there refer to the lowest three levels for each of the systems. The importance of the anisotropic potential couplings which pertain to $\Delta\lambda = 2$ and $\Delta\lambda = 4$, as clearly seen from the panels of Figure 2, is once more causing the $(4 \rightarrow 2)$ transitions to provide the largest de-excitation rates in the examined temperature range. Furthermore, the difference in size between the $(2 \rightarrow 0)$ and the $(4 \rightarrow 0)$ rates indicates the different strengths between the two direct couplings which chiefly control those transitions. Additionally, we see that the o-D_2^+ system always yields smaller relaxation rates with respect to the H_2^+ system, although the relative differences decrease when the Δj values increase: it indicates that the reduced strength of the coupling for the larger lambda coefficients is offsetting the expected increase in the dynamical efficiency originating from the reduction of the energy gaps between the two systems.

The same comparison of de-excitation rates is presented in the right panel of the same Figure 5, involving however the p-H_2^+ and the HD^+ systems. The differences already discussed earlier between their computed de-excitation cross sections is now reflected by the differences exhibited by their corresponding relaxation rates: although the kinematic effects favour the energy transfers within the levels of the lighter isotope, the changed symmetry of the HD^+ produces a larger number of accessible levels. Hence, the $(4 \rightarrow 2)$ transition produces much larger de-excitation rates for the H_2^+ target, while the HD^+ system can also depopulate that initial level via the $(4 \rightarrow 3)$ and the $(4 \rightarrow 1)$ transitions which are absent for H_2^+. Additionally, we see that the rates for the $\Delta j = 4$ transitions, involving larger, and weaker, anisotropic PES coefficients in both cases, are now comparable in the two isotopes and much smaller than the previous de-excitation rates. One can therefore argue from this specific region of levels that the greater number of relaxation paths available to the HD^+ system is causing an overall greater efficiency of collisional depopulation of the higher excited rotational levels of this system in comparison with the former.

5 Computing the relaxation times from the master equations

The calculations for the time evolution of the rotational populations of all the present molecular ions are presented below.

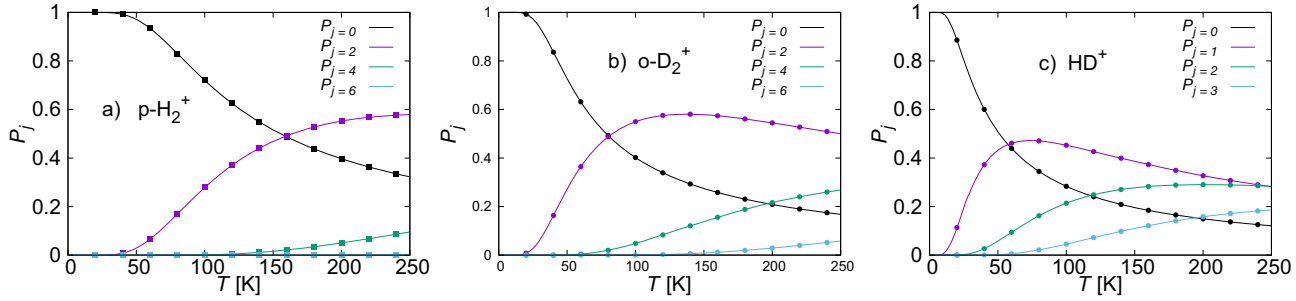

Fig. 6. Steady-state solution of the rate equations for p-H_2^+, o-D_2^+ and HD^+ as a function of collisional temperature. In this calculations we do not include the spontaneous downward relaxation rates of HD^+. Continuous lines are the computed solutions using a SVD technique. The points correspond to the Boltzmann distribution.

The relevant rate coefficients allow us to compute the cooling dynamics using conventional rate equations:

$$d\mathbf{p}(t)/dt = n_{\rm He}\mathbf{K}(T)\cdot\mathbf{p}(t), \qquad (3)$$

where the quantity $n_{\rm He}$ is the selected value of the density of the He buffer gas, the elements of the vector $\mathbf{p}$ are the time-evolving (from initial to final) fractional rotational populations $p_j(t)$, and $\mathbf{K}(T)$ is the matrix including all the relevant inelastic rate coefficients of the problem,

$$\mathbf{K} = \begin{pmatrix} -\sum_{i=2}^{n} k_{1,i} & k_{2,1} & \cdots & k_{n,1} \\ k_{1,2} & -\sum_{i=1,\neq 2}^{n} k_{2,i} & & \vdots \\ \vdots & & & \\ k_{1,n} & \cdots & & -\sum_{i=1}^{n-1} k_{n,i} \end{pmatrix}.$$

The cases of the three isotopic variants are treated separately since, as mentioned earlier, there are no interconversion processes involving them. The initial conditions $\mathbf{p}(t=0)$ and the collisional temperature T corresponding to the mean collisional energy must be chosen according to the existing experimental conditions selected and the present specific choices will be indicated below.

In the limit of negligible kinetic temperature of the MHI, the collisional temperature is related to the temperature of the He buffer gas by $T = \frac{m_{\rm ion}}{m_{\rm He}+m_{\rm ion}} T_{\rm He}$.

It is known that the MHIs produced by electron impact ionization are obtained over a large range of vibrational and rotational levels: for a recent discussion see [13]. We further consider in the present relaxation model that the molecular ions have already reached their lowest vibrational levels and that only the lower rotational levels are populated for each of them. We use this assumption because the main task here is to compare the three variants in order to obtain estimates of the different rotational relaxation times linked to their structural differences analyzed before.

In order to compare the buffer gas cooling effects, we assume a high initial rotational temperature $T_{rot} = 400$ K and choose the values of $p_j(t=0)$ according to the Boltzmann distributions of the MHIs within their individual rotational levels. For the sake of our comparative study, it will be sufficient to consider levels up to $j = 10$ for each of the MHIs studied here.

If the rate coefficients satisfy the detailed balance relations, the solution of equation (3) will approach, as $t \to \infty$, the Boltzmann distribution associated with the temperature of the He buffer gas. This asymptotic solution corresponds to the steady-state solution of the rate equations, and they may be computed setting $d\mathbf{p}(t)/dt = 0$ and solving the resulting homogeneous equations. We solved these homogeneuos equations by using the singular value decomposition technique (SVD) [23]. We further verified that the solutions coincide with the Boltzmann distribution when $t \to \infty$ for each of the present systems, see Figure 6.

The following additional comments can be made about the data in Figure 6, where we present the steady-state solutions of the rate equations as a function of the collisional temperature for all the three systems of the present study:

(i) when we focus on a specific low temperature of, say $T = 20$ K, then we see that the lightest isotope is the one which has reached a population of its $j = 0$ level which is very close to 100% while all other excited levels carry very negligible populations;

(ii) in the case of the heaviest isotope, the D_2^+ system, we see instead that, at 30 K the population of its lowest rotational level is slightly lower, around 75%, while the population of its next level $j = 1$ has become, while still small, as large as 25%.

A further indication of the relative efficiencies of the relaxation processes at the lower temperatures can be gleaned from the temporal evolution data presented in the panels of Figure 7.

At $t = 0$, the rotational level population are described by a Boltzmann distribution at 400 K and their temporal propagation was carried out by solving equation (3) using the Runge-Kutta method. Within the rate equations for the HD^+ isotope we have specifically included the spontaneous downward relaxation rates computed by Coppola et al. [24]. Figure 7a compares the temporal evolutions of the first three levels of p-H_2^+ (solid lines) with those for o-D_2^+ (dashed lines) at the lowest temperature examined of $T = 10$ K. The same slower evolution of the relaxation of level populations of o-D_2^+ compared with those of the lighter molecular ion is clearly seen from the data. It takes between 3 s and 4 s for the p-H_2^+ to decay almost 100%

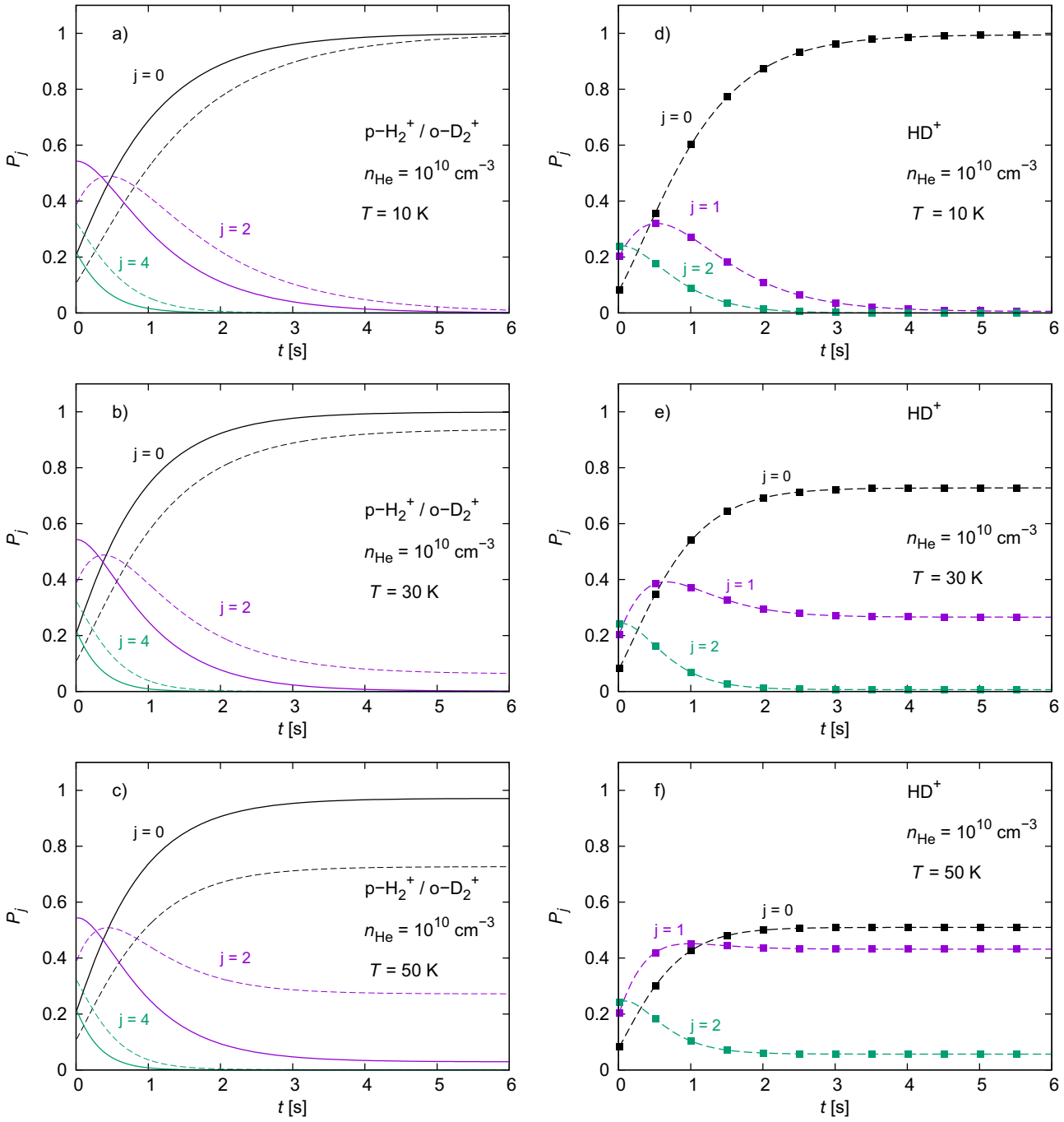

Fig. 7. Left panels: temporal evolution of the rotational level populations of p-H_2^+ (continuous lines) and o-D_2^+ (dotted lines). Right panel: the same for HD^+. The He density was 10^{10} cm^{-3} in all cases.

into its $j = 0$ state, while the o-D_2^+ system needs more than 6 s to reach the same dominant population of its ground rotational state.

As the temperature is increased to 30 K (Fig. 7b) and to 50 K (Fig. 7c) we clearly see that the differences in the speed of the temporal relaxation into the lowest rotational levels of the two homonuclear isotopes become even more marked. If we focus, as an example, at the $t = 3$ s time interval we see that at the highest temperature presented in the Figure, the D_2^+ molecular ion has only reached a population of less than 65% into its $j = 0$ state, with a large population still present in the $j = 2$ state.

The data in Figures 7d to 7f refer exclusively to the temporal evolutions of the HD^+: we see in this case that only at the lowest collision temperature of 10 K the molecular ion reaches, after about 6 s, a rotational population of its lowest rotational state of nearly 100%. However, as the temperature increases up to 50 K, only about 40% of the state population is in the $j = 0$ level, thereby pointing at a slower progression to equilibrium for the polar MHI.

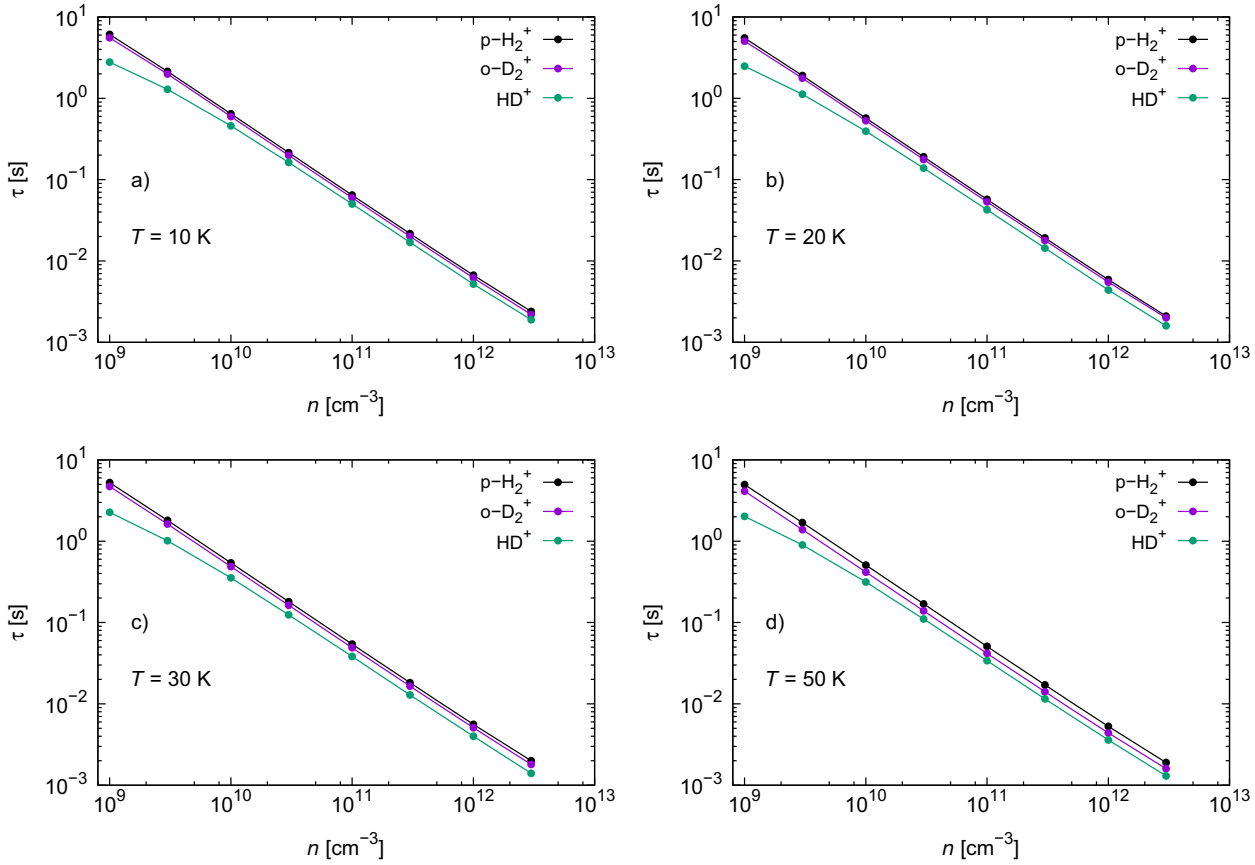

Fig. 8. Cooling times as a function of He density and for different temperatures in the trap. Both axes are shown in a logarithmic scale.

We define the cooling time/τ to be given by the following relation:

$$\langle E_{rot}\rangle(\tau) = \langle E_r\rangle(t\to\infty) + \frac{1}{e}(\langle E_r\rangle(t=0) - \langle E_r\rangle(t\to\infty)) \quad (4)$$

where τ corresponds to the cooling time at $1/e$ of the average rotational energy, where e is the Euler number. One can then examine the behavior for all the MHIs discussed in this work, comparing them as a function of the buffer gas properties, as shown below.

The results from the present calculations are reported in Figure 8. We have included in the calculations for the HD^+ system the effects coming from the spontaneous radiative cooling of the polar system. As discussed earlier, such effects are particularly important at very low densities of the buffer gas since then their rates become competitive with the collisional rates. The data of Table 2 compare the radiative rates with the collisional ones at two different temperatures and for a specific choice of the He gas density. If, for example, we focus on the $j = 0$ situations, we see there that a reduction of the buffer gas density by one or two orders of magnitudes will bring the collisional rates down to the values of the radiative rates. Thus, we can argue that the competition would be significant only at the lower densities of the buffer gas. We can therefore see in all panels of Figure 8 that, at the lower densities for the He buffer gas, the contributions from the spontaneous radiative cooling of HD^+ causes a change in the $1/n_{He}$ behaviour. We can also briefly comment on the data reported in the figure, where the trap temperatures vary from the lowest one of 10 K to the highest one of 50 K in Figure 8d:

(i) at the lowest temperature of 10 K, and for a He density of 10^{10} cm^{-3}, we see that for the HD^+ partner ion the cooling time has a value of about 0.5 s while the other two molecules exhibit slightly longer cooling times of about 0.6 s for ortho-D_2^+ and 0.7 s for para-H_2^+. Such small differences would not be relevant at the experimental level;

(ii) at the highest temperature considered, i.e. the data of Figure 8d, we see that the HD^+ cooling time, at the same He gas density of the previous example, is about 0.3 s while the cooling time for ortho-D_2^+ and para-H_2^+ are of 0.4 s and 0.5 s respectively. Here again such small variations will not affect the experiment.

One should also note at this point that the present study is chiefly focussed on a comparative analysis of the collisional relaxation times between three different isotopologues of molecular MHIs. As such, the use of the simplified angular momentum coupling which we have used to generate the relevant rates would have a marginal effect on our final results. Judging from the differences in the cross section

Table 2. Comparison between the spontaneous downward rates and the cooling collisional rates of HD^+ at two different temperatures and at $n_{He} = 10^9$ cm^{-3}. The units are s^{-1}.

Transition		$T = 10$ K	$T = 30$ K
$j \to j'$	$A_{j\to j'}$	$n_{He} \times k_{j\to j'}$	$n_{He} \times k_{j\to j'}$
$1 \to 0$	0.0066	0.137	0.139
$2 \to 1$	0.0634	0.181	0.224
$3 \to 2$	0.2268	0.149	0.205
$4 \to 3$	0.5497	0.148	0.180
$5 \to 4$	1.0786	0.136	0.171
$6 \to 5$	1.8517	0.105	0.145
$7 \to 6$	2.8985	0.125	1.494
$8 \to 7$	4.2383	0.127	1.489
$9 \to 8$	5.8881	0.103	0.127
$10 \to 9$	7.8257	0.103	0.125

values shown partially in Table 1, in fact, the accurate rates would be only a few percent larger than the present ones. Such differences would not change the relative scaling and the overall comparative behaviour of the results we have discussed in Figure 8.

6 Present conclusions

We have carried out in the present study a detailed comparison of the quantum dynamical processes which are linked to the internal energy relaxation times of three different MHIs interacting with He buffer gas under cryogenic temperature conditions. In particular, we have presented a model study in which the partner molecular ions are considered to have already undergone faster relaxation processes in the trap (also via collisions with He gas) and have reached their ground vibrational levels. As a next step, they further undergo internal relaxation from their lower rotational levels into their ground rotational states by collisional processes involving again He atoms.

To this end, we have first carried out accurate quantum scattering calculations to obtain the state-to-state de-excitation and excitation cross sections over a broad range of collision energies. A detailed comparison of the different behavior shown by the molecular ions being considered, i.e. para-H_2^+, ortho-D_2^+ and HD^+, indicates already that specific structural features of their interaction potentials play a significant role in changing the relative sizes of such cross sections, where the differences in the rotational level spacings are also contributing to provide different cross section values.

We have also generated the corresponding state-changing rates over a range of temperatures up to about 100 K and employed them within the solutions of the kinetic equations that control the time evolutions of the rotational state populations of the three molecules. They were assumed to have an initial internal temperature of about 400 K in order to clearly display the time evolution behaviour down to their ground rovibrational states.

In order to model possible future experiments, we have may consider a density of the buffer gas such that the mean time between collisional events is smaller that the spectroscopic cycle time. As discussed elsewhere [25] we may consider this time to be around 1 s for all three systems, so that the density is approximately 1×10^9 cm^{-3}. Under this condition, the calculations indicate for all three systems mean cooling times between 4 s and 7 s, which is a reasonable request for the trap's experimental conditions.

We further found that the differences in the density of rotational states per unit of energy clearly affect the cooling times: the HD^+ shows the shortest cooling times at all temperatures.

We have therefore shown that using accurate interaction potentials, coupled with exact quantum scattering dynamics, can achieve a realistic modeling of the relaxation times for simple molecular ions in traps and can provide useful indications for the setting up of experimental manipulations.

This work has been made possible by the COMIQ Marie Curie Initial Training Network FP7-PEOPLE-2013-ITN: COMIQ: Cold Molecular Ions at the Quantum limit funded by the European Commission under the Grant Agreement 607491. It has supported all the research groups authoring this paper. The Innsbruck group also acknowledges support by the Austrian Science Fund FWF, Project No. P27047-N20. The computational results presented in this work have been achieved (in part) using the HPC infrastructure LEO of the University of Innsbruck. Open access funding provided by Institut für Ionenphysik und Angewandte Physik.

Author contribution statement

All authors have contributed equally to the completion of the present work.

References

1. S. Willitsch, M.T. Bell, A.D. Gingell, T.P. Softley, Phys. Chem. Chem. Phys. **10**, 7200 (2008)
2. A. Harter, J. Hecker Denschlag, Contemporary Physics **55**, 33 (2014)
3. F.H.J. Hall, P. Eberle, G. Hegi, M. Raoult, M. Aymar, O. Dulieu, S. Willitsch, Molecular Physics **111**, 2020 (2013)
4. F.H.J. Hall, S. Willitsch, Phys. Rev. Lett. **109**, 233202 (2012)
5. E.R. Hudson, Phys. Rev. A **79**, 032716 (2009)
6. A.K. Hansen, O.O. Versolato, Ł. Kłosowski, S.B. Kristensen, A. Gingell, M. Schwarz, A. Windberger, J. Ullrich, J.R.C. López-Urrutia, M. Drewsen, Nature **508**, 76 (2014)
7. D. Gerlich, R. Plasil, I. Zymak, M. Hejduk, P. Jusko, D. Mulin, J. Glosk, J. Phys. Chem. A **117**, 10068 (2013)
8. P. Jusko, O. Asvany, A.-C. Wallerstein, S. Brünken, S. Schlemmer, Phys. Rev. Lett. **112**, 253005 (2014)

9. D. Hauser, S. Lee, F. Carelli, S. Spieler, O. Lakhmanskaya, E.S. Endres, S.S. Kumar, F. Gianturco, R. Wester, Nature Physics **11**, 467 (2015)
10. S. Schiller, V. Korobov, Phys. Rev. A **71**, 032505 (2005)
11. U. Bressel, A. Borodin, J. Shen, M. Hansen, I. Ernsting, S. Schiller, Phys. Rev. Lett. **108**, 183003 (2012)
12. T. Schneider, B. Roth, H. Duncker, I. Ernsting, S. Schiller, Nat. Phys. **6**, 275 (2010)
13. M. Hernández Vera, F.A. Gianturco, R. Wester, H. da Silva Jr., O. Dulieu, S. Schiller, J. Chem. Phys. submitted, (2016)
14. M.F. Falcetta, P.E. Siska, Mol. Phys. **97**, 117 (1999)
15. Ashwani Kumar Tiwari, N. Sathyamurthy, J. Phys. Chem. A **110**, 11200 (2006)
16. C.N. Ramachandran, D. De Fazio, S. Cavalli, F. Tarantelli, V. Aquilanti, Chem. Phys. Lett. **469**, 26 (2009)
17. I. Iskandarov, H. Da Silva Jr., M. Hernández Vera, F.A. Gianturco, O. Dulieu, R. Wester, Eur. Phys. J. D, in preparation (2016)
18. R. Taylor, *The Quantum Theory of nonrelativistic Collisions* (New York, Dover, 2006)
19. D. López-Durán, E. Bodo, F.A. Gianturco, Comput. Phys. Commun. **179**, 821 (2008)
20. D.E. Manolopoulos, J. Chem. Phys. **85**, 6425 (1986)
21. J.Ph. Karr, L. Hilico, J. Phys. B: At. Mol. Opt. Phys. **39**, 2095 (2006)
22. S. Stimson, M. Evans, C.-W. Hsu, C.Y. Ng, J. Chem. Phys. **126**, 164303 (2007)
23. W.H. Press, S.A. Teukolsky, W.T. Vetterling, B.P. Flannery, Numerical Recipes in FORTRAN; The Art of Scientific Computing, 2nd edition (Cambridge University Press, New York, NY, USA, 1993)
24. C.M. Coppola, L. Lodi, J. Tennyson, MNRAS **415**, 487 (2011)
25. S. Schiller, I. Kortunov, M. Hernández Vera, H. Da Silva Jr., F.A. Gianturco, Phys. Rev. A, submitted, (2017)